Please cite the Published Version

Data Access Statement: The data that support the findings of this study are available from the corresponding author upon reasonable request.

Prominent Structural Dependence of Quantum Capacitance Unraveled by Nitrogen-Doped Graphene Mesosponge

Rui Tang,* Alex Aziz, Wei Yu, Zheng-Ze Pan, Ginga Nishikawa, Takeharu Yoshii, Keita Nomura, Erin E. Taylor, Nicholas P. Stadie, Kazutoshi Inoue, Motoko Kotani, Takashi Kyotani, and Hirotomo Nishihara*

Porous carbons are important electrode materials for supercapacitors. One of the challenges associated with supercapacitors is improving their energy density without relying on pseudocapacitance, which is based on fast redox reactions that often shorten device lifetimes. A possible solution involves achieving high total capacitance (C_{tot}), which comprises Helmholtz capacitance (C_H) and possibly quantum capacitance (C_Q), in high-surface carbon materials comprising minimally stacked graphene walls. In this work, a templating method is used to synthesize 3D mesoporous graphenes with largely identical pore structures ($\approx$2100 m^2 g^{-1} with an average pore size of $\approx$7 nm) but different concentrations of oxygen-containing functional groups (0.3–6.7 wt.%) and nitrogen dopants (0.1–4.5 wt.%). Thus, the impact of the heteroatom functionalities on C_{tot} is systematically investigated in an organic electrolyte excluding the effect of pore structures. It is found that heteroatom functionalities determine C_{tot}, resulting in the cyclic voltammetry curves being rectangular or butterfly-shaped. The nitrogen functionalities are found to significantly enhance C_{tot} owing to increased C_Q.

1. Introduction

Supercapacitors are promising energy storage devices with outstanding power outputs ($\approx$15 kW kg^{-1})[1] and long life cycles ($>$1 000 000 cycles),[2] rendering them fascinating candidates for military, satellite, electric vehicle, and microgrid applications.[3] However, the energy densities of supercapacitors tend to be relatively low ($\approx$10 Wh kg^{-1}), making them unsuitable for energy-demanding applications.[4] The key components of supercapacitors include electrode materials, a separator, electrolyte, and current collectors. As previously reported, one potential avenue to increase the energy density of supercapacitors is to increase the total capacitance (C_{tot}) of the porous carbon material used as the electrode material.[1] Furthermore, relying on pseudocapacitance, which originates from fast redox reactions that lead to shorter device lifetimes, is not preferable. One approach for enhancing C_{tot} is to increase the contribution of one or more of its individual components: Helmholtz capacitance (C_H), diffuse layer capacitance (can be ignored in the presence of a concentrated electrolyte),[5] and possibly quantum capacitance (C_Q).[6] Understanding the nature of these capacitance contributions is fundamental to various fields, including electrochemistry, energy storage, and

R. Tang
College of Materials Science and Engineering
Hunan Joint International Laboratory of Advanced Materials and Technology for Clean Energy
Hunan Province Key Laboratory for Advanced Carbon Materials and Applied Technology
Hunan University
Changsha 410082, China
E-mail: tangrui01@hnu.edu.cn
R. Tang, A. Aziz, W. Yu, Z.-Z. Pan, K. Inoue, M. Kotani, H. Nishihara
Advanced Institute for Materials Research (WPI-AIMR)
Tohoku University
2-1-1 Katahira, Aoba-ku, Sendai 980–8577, Japan
E-mail: hirotomo.nishihara.b1@tohoku.ac.jp

The ORCID identification number(s) for the author(s) of this article can be found under https://doi.org/10.1002/smll.202308066

A. Aziz
International Research Fellow of Japan Society for the Promotion of Science (Postdoctoral Fellowships for Research in Japan)
Tokyo Japan
G. Nishikawa, T. Yoshii, K. Nomura, E. E. Taylor, T. Kyotani, H. Nishihara
Institute of Multidisciplinary Research for Advanced Materials
Tohoku University
2-1-1 Katahira, Aoba-ku, Sendai 980–8577, Japan
E. E. Taylor, N. P. Stadie
Department of Chemistry & Biochemistry
Montana State University
Bozeman, Montana 59717, USA

**ADVANCED
SCIENCE NEWS**

www.advancedsciencenews.com

NANO · MICRO

small

www.small-journal.com

electrocatalysis.[6] Thus, research on carbon materials has focused on the origin of C_{tot}, its determinants, how it can be improved, and the reason why C_{tot} sometimes varies depending on the applied potential.[6,7]

To maximize C_H, the graphene walls of porous carbon materials should be minimized to increase specific surface area (SSA). However, minimally stacked graphene walls often display a capacitance drop near their potential at zero charge, resulting in an inferior C_{tot}.[8] Therefore, it is crucial to elucidate the key factors that increase C_{tot} in high-SSA carbon materials with minimally stacked graphene walls, including highly activated carbons, single-walled carbon nanotubes, and graphene-based porous materials. Due to their structural complexity, porous carbon materials' structure-capacitance relationship has not been thoroughly investigated.[9] The structural features of these materials include SSA, pore size and shape, topological defects, edge sites, and heteroatoms.[9] The SSA is determined by the basal plane and edge sites of the porous carbon material.[10] Pores can be classified as micropores (< 2 nm), mesopores (2–50 nm), and macropores (> 50 nm),[11] and can be open or closed depending on how they are connected. Topological defects are typically non-hexagonal carbon ring structures, such as five-, seven-, and eight-membered rings in the graphene basal plane.[12] Edge sites are more complex; various types have been reported thus far including triplet carbenes and σ-radicals (doublet), which could exist as dangling bonds, σ-radicals at H-terminated zigzag edge sites, H-terminated armchair edge sites, hydroxyl, acid anhydride, lactone, carboxyl, carbonyl, and ether groups.[13] Heteroatoms can be also incorporated into carbon frameworks. For example, nitrogen doping allows for the incorporation of various nitrogen species, including pyridine N-oxide, pyridinic, pyrrolic, and graphitic nitrogen. This broad array of possible structural features and the corresponding subtle or substantial variations in their chemical properties add to the complexity of the porous carbon materials.

Various competing theories have been proposed to gain insights into the complexity of porous carbon materials. However, far from providing some clarity, these theories have instead often spawned conflicting claims. Regarding the basal plane, one well-known theory has supported the concept of space charge capacitance (C_{SC}).[14–16] Specifically, it proposes that C_{SC} is determined by the basal plane thickness and is dependent on the potential.[17] Although such a theory may qualitatively explain the low value of C_{areal} (C_{tot} per SSA) and the observation of butterfly-shaped cyclic voltammetry (CV) curves, a quantitative analysis of these curves remains to be seen.[18,19] Another theory incorporates C_Q, which has been used to quantitatively explain the variation in the C_{tot} of graphene at different potentials.[20] Graphene's C_{tot} is generally considered to be primarily determined by C_H and by C_Q.[20–24] The origin of C_Q can be understood as follows: graphene is not a conductor, but a semiconductor. When ions with a charge of Q are electrostatically adsorbed on graphene, in addition to the potential change (U_H) caused by band shift relative to the neutral surface, there is also a potential change (U_Q) caused by the Fermi level shift relative to the Dirac point.[25] Therefore, according to the definition of total capacitance (C_{tot}), $C_{tot} = Q/(U_H + U_Q)$, inverting the above equation yields: $1/C_{tot} = U_H/Q + U_Q/Q = 1/C_H + 1/C_Q$.[25] However, a C_Q-based theory falls short of being a general theory that satisfactorily ex-

plains much of the experimental data encompassing a gamut of materials ranging from graphene to porous carbon materials. For example, the CV curves of most porous carbon materials have not displayed any features attributable to C_Q. In addition, no report has offered direct evidence that connects the enhanced C_{tot} of modified porous carbon materials to a corresponding gain in C_Q.[22,26] Therefore, the C_Q theory has received only limited acceptance from researchers involved in porous carbon materials research,[6,7] despite the fact that graphene is a component of porous carbon materials. Furthermore, it has been proposed that ion reorganization within an electrolyte, rather than the electronic properties of carbon materials (C_{SC} or C_Q), underpin the C_{tot} variation under different potentials.[27] Regarding edge sites, one well-known theory is based on pseudocapacitance, which typically originates from reversible redox reactions between oxygen[28–30] or nitrogen functionalities[31] and an aqueous electrolyte. Note that pseudocapacitance is often used to express capacitance enhancement for unknown reasons.[32] Other theories propose that the presence of oxygen functionalities enhances C_H by improving the wettability[29] or carbon-ion interaction.[33] In terms of pore size, ions' inability to penetrate small pores has been cited to explain the decrease in C_{tot}.[34] Such an explanation is sometimes used to explain the low value of C_{areal} for activated carbon materials with high SSAs.[35] On the other hand, an increase in C_{areal} has been observed when the pores and ions have matching sizes;[36,37] however, the mechanism behind the observed increase in C_{areal} remains elusive.[38–41] Additionally, it has been proposed that the butterfly shape of certain CV curves might be due to the electrowetting of the smallest pores.[42] Nitrogen doping has also been demonstrated to enhance C_{tot} by introducing pseudocapacitance,[43,44] improving wettability,[45] enhancing carbon-ion interaction,[33,46] or increasing C_Q.[22,47] However, some researchers disagree with the notion that nitrogen doping can enhance C_{tot}. It is reported that nitrogen doping is not so effective in enhancing C_{tot}[1] or even negatively affects C_{tot} at high current densities in organic electrolyte-based supercapacitors.[48]

To facilitate the development of a C_{tot} theory for porous carbon materials and elucidate the structure-capacitance relationship in high-surface carbon materials with minimally stacked graphene walls, one approach is to initially design or use carbon materials with fixed or relatively simple structural features and potentially branch out later to carbon materials with more complex structures. We recently reported that a C_Q-based theory, rather than one based on C_{SC}, can explain the capacitance behavior of an edge-site-free three-dimensional mesoporous graphene prepared using a template carbonization method.[8] This carbon material was named graphene mesosponge (GMS) because of its uniform sponge-like mesoporous structure, essentially a negative replica of a sacrificial template of Al_2O_3 nanospheres ($\phi = \approx 7$ nm).[49] GMS is a powdery form with a particle size of $\approx 10\,\mu m$, and its SSA is as high as $\approx 1900\ m^2\ g^{-1}$. Moreover, GMS exhibits a capacitance performance closer to that of graphene due to its specific framework with minimally stacked basal planes and very few edge sites. Here, we report the preparation of nitrogen-doped graphene mesosponge (N-GMS) via chemical vapor deposition (CVD) on a sacrificial template of Al_2O_3 nanospheres ($\phi = \approx 7$ nm). We show that the investigation of any capacitance performance variations or similarities among graphene and its

ADVANCED
SCIENCE NEWS
www.advancedsciencenews.com

NANO · MICRO
small
www.small-journal.com
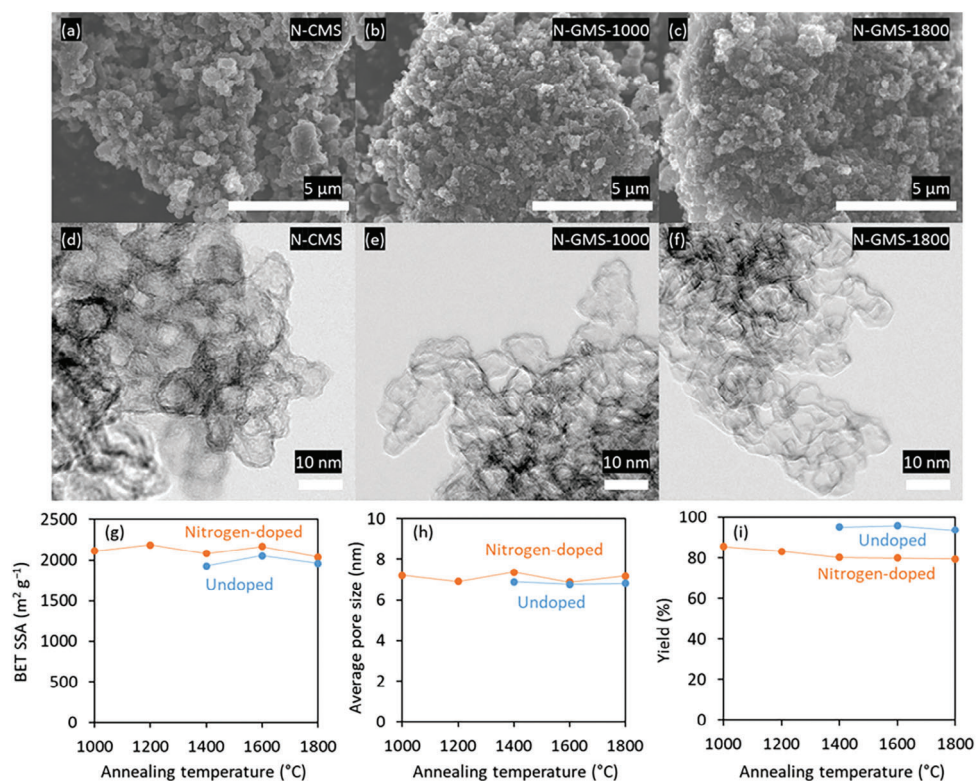
Figure 1. a–c) SEM and d–f) TEM images of the nitrogen-doped carbon species: (a,d) N-CMS, (b,e) N-GMS-1000, and c,f) N-GMS-1800. g) BET SSAs and h) average pore sizes of the carbon materials after high-temperature annealing. i) Carbon yields after high-temperature annealing for the doped and undoped materials.

3D frameworks is enabled using a series of N-GMS materials as models. We also propose intrinsic mechanisms by which oxygen-containing functional groups and nitrogen doping affect C_Q and C_{tot}. Ultimately, these investigations aim to break through the low energy density bottleneck that has hindered progress in the field of supercapacitors.

2. Results

GMS can be synthesized by high-temperature annealing of its precursor, carbon mesosponge (CMS). CMS was synthesized by methane CVD at 900 °C for 100 min on a sacrificial template of Al_2O_3 nanospheres ($\phi = \approx 7$ nm). **Figure 1a** shows a scanning electron microscopy (SEM) image of the nitrogen-doped carbon mesosponge (N-CMS) synthesized by acetonitrile CVD at 650 °C for 3 h on the same Al_2O_3 templates. Acetonitrile was used as the source of both carbon and nitrogen (see the Experimental Section and Figure S1, Supporting Information). Nearly one carbon layer was deposited, as confirmed by thermogravimetric (TG) analysis (Figure S2, Supporting Information). The resulting material exhibited a particle size of ≈ 10 μm. These relatively large particles were found to be composed of smaller aggregated particles. In addition, numerous macropores were observed on the particle surfaces. Following high-temperature annealing of the prepared N-CMS from 1000 to 1800 °C, we synthesized a series of samples denoted N-GMS-1000, N-GMS-1200, N-GMS-1400, N-GMS-1600, and N-GMS-1800, where the number indicates the corresponding annealing temperature. The morphologies of the samples were found to be very similar (see, for example, Figure 1b,c). Furthermore, the samples comprised hollow spheres with a diameter of ≈ 7 nm and were essentially negative replicas of the Al_2O_3 template, as shown in the transmission electron microscopy (TEM) images of the pristine and annealed nitrogen-doped carbon materials (Figure 1d–f). As shown in Figure S3a (Supporting Information), the type IV nitrogen adsorption–desorption isotherms and hysteresis at $P/P_0 > 0.4$ indicate the presence of a highly mesoporous structure for the pristine and annealed carbon species. A slight increase is shown at P/P_0 greater than 0.95 meaning some macropores in these carbon materials.[50–52] The Brunauer–Emmett–Teller (BET) surface areas (S_{BET}) of N-CMS, N-GMS-1000, N-GMS-1200, N-GMS-1400, N-GMS-1600, and N-GMS-1800 were determined to be 2369, 2112, 2186, 2079, 2116, and 2037 m^2 g^{-1}, respectively. Although the SSA of N-CMS was slightly higher than the annealed samples probably due to its larger number of edge sites, the SSA of the annealed samples are almost identical up to 1800 °C (Figure 1g).

The samples prepared with a shorter CVD time of 1 h showed significantly reduced S_{BET} after high-temperature annealing (Figure S4, Supporting Information), suggesting that CVD time is a critical parameter for controlling the robustness of the prepared carbon frameworks. In general, high-temperature annealing of porous carbon materials has been found to be detrimental to their porous structures.[53] However, we previously synthesized a series of templated mesoporous carbon materials that were able to withstand high-temperature annealing up to 1800 °C
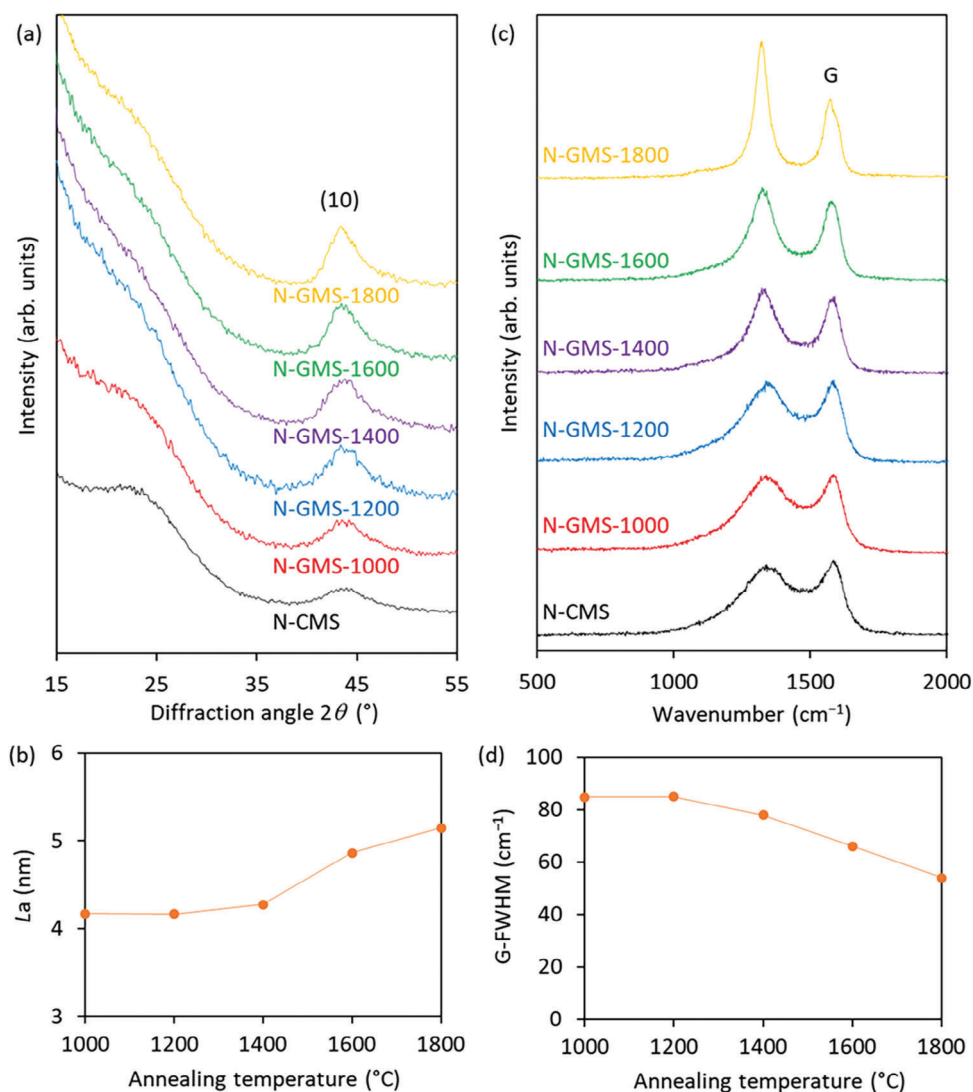
ADVANCED
SCIENCE NEWS

www.advancedsciencenews.com

NANO · MICRO

small

www.small-journal.com
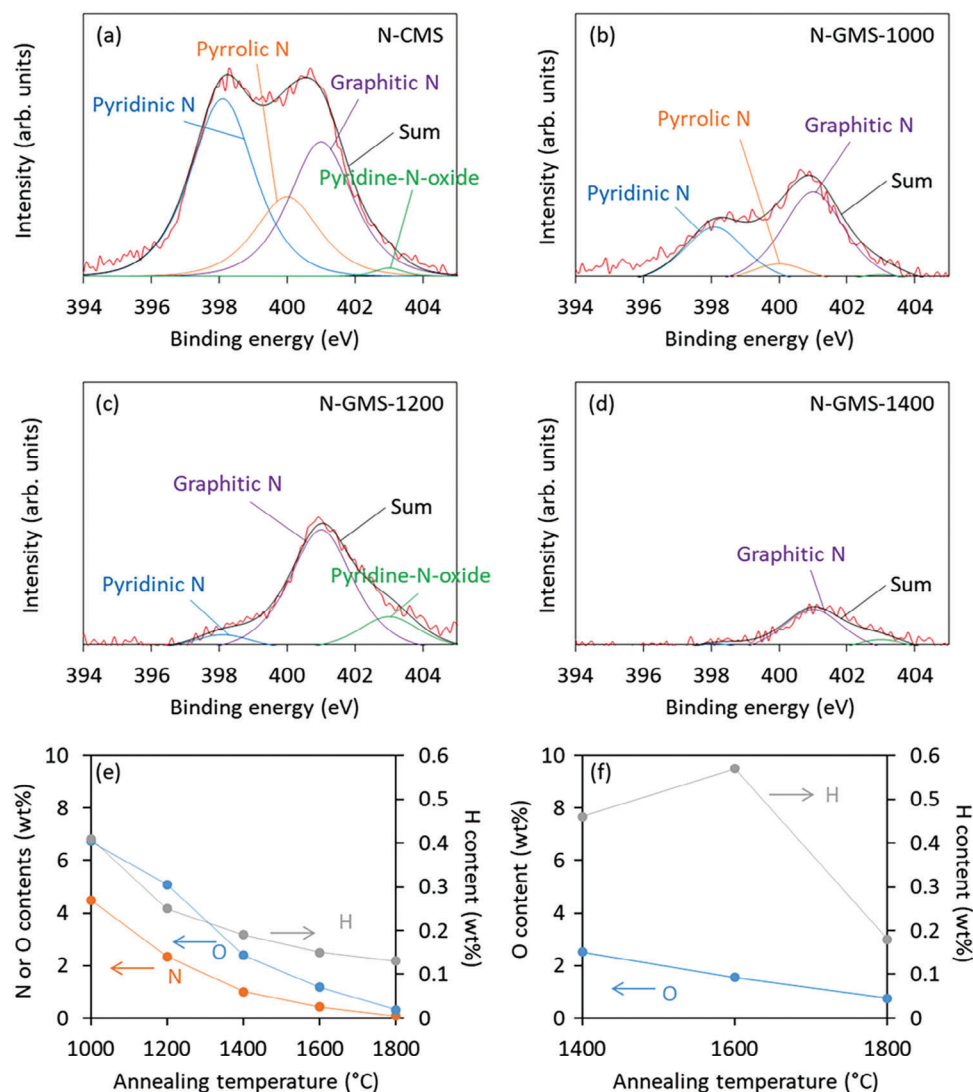
Figure 2. N1s XPS results for the a) N-CMS, b) N-GMS-1000, c) N-GMS-1200, and d) N-GMS-1400. Elemental analysis results for the e) doped and f) undoped carbon materials.

without significant alteration in their pore structures.[49,54,55] This work, therefore, extends our earlier templating method to preparing nitrogen-doped mesoporous carbon materials. Indeed, in addition to the SSAs, the pore-size distributions (Figure S3b, Supporting Information) and average pore sizes (Figure 1h) of the annealed materials were nearly identical, suggesting that the carbon frameworks were largely retained after high-temperature annealing. Thus, using N-GMSs as model materials allowed us to achieve nearly unchanged SSA and pore size distribution, which facilitated the elucidation of C_{tot}.

We also synthesized an undoped carbon mesosponge (CMS) via CVD at 900 °C for 100 min using the same sacrificial template and methane as the carbon source (see the Experimental Section in the Supporting Information). As with the nitrogen-doped sample, nearly one carbon layer was deposited, as verified by TG results (Figure S5, Supporting Information). We also subjected CMS to high-temperature annealing at 1400, 1600, and 1800 °C; the resulting carbon specimens were denoted GMS-

1400, GMS-1600, and GMS-1800, respectively. These undoped carbon materials possess pore structures similar to those of the nitrogen-doped carbon materials (Figure 1g,h) and were considered suitable reference materials. The carbon yields after high-temperature annealing (Figure 1i) were slightly lower in the nitrogen-doped samples (79.4–85.5 wt.%) than in the undoped species (93.6–95.8 wt.%) because of the thermal decomposition of the nitrogen and oxygen functionalities, as will be demonstrated later.

Figure 2a–d show the X-ray photoelectron spectroscopy (XPS) profiles of the nitrogen-doped carbon materials. The N 1s peak is deconvoluted into four peaks according to the literature.[56–60] N-CMS shows three major N 1s peaks at 401, 400, and 398 eV, corresponding to graphitic N, pyrrolic N, and pyridine N, respectively, and a minor peak at 403 eV, corresponding to pyridine N-oxide (Figure 2a).[56,57] With increasing the annealing temperature, the peak intensity decreased due to the thermal decompositions of the N-species, and only the graphitic N remained at 1400 °C due
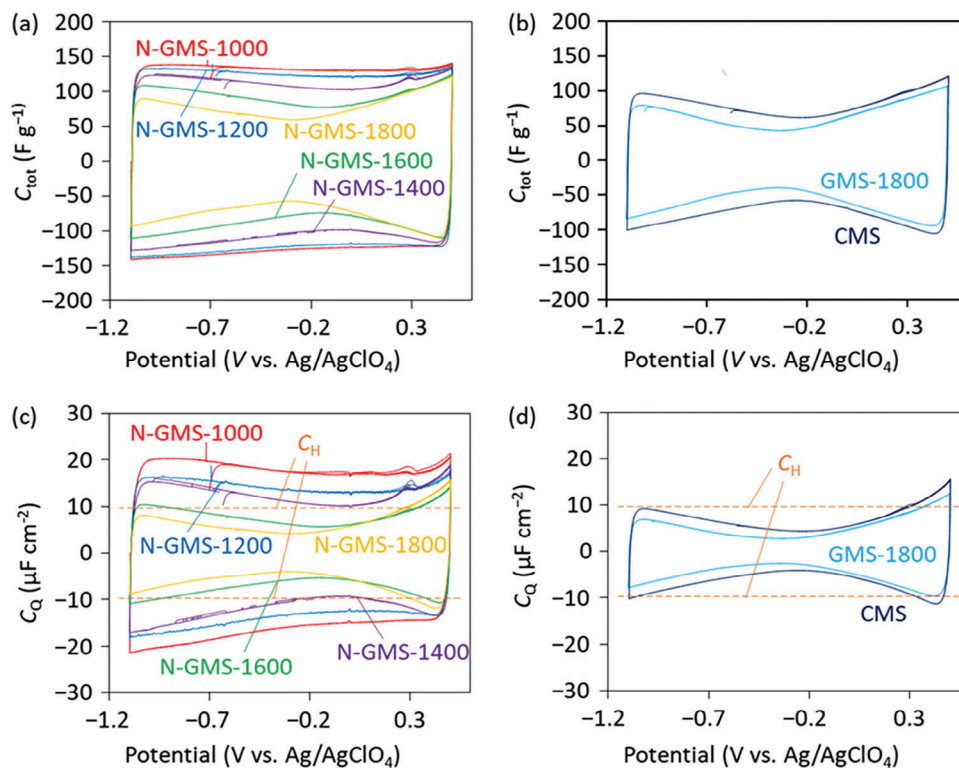
**ADVANCED
SCIENCE NEWS**

www.advancedsciencenews.com

**NANO · MICRO
small**

www.small-journal.com

Figure 3. a) XRD results, b) L_a, c) Raman results, and d) G-FWHM for the nitrogen-doped carbon materials.

to its higher stability than the other nitrogen compounds.[61,62] After annealing at 1600 and 1800 °C, no N 1s signal was detected by XPS. Figure 2e,f show the bulk elemental (CHN) analysis results for the nitrogen-doped and undoped carbon materials. Upon increasing the annealing temperature from 1000 to 1800 °C, the amount of nitrogen gradually decreased from 8.3 wt.% (N-CMS) to 4.5, 2.4, 1.0, 0.4, and 0.1 wt.% (Figure 2e). At the same time, the O content also decreased from 9.3 wt.% (N-CMS) to 6.7, 5.1, 2.4, 1.2, and 0.3 wt.%. The results shown in Figures 1 and 2 indicated that the surface of the nitrogen-doped carbon specimen can be converted from highly functionalized (8.3 wt.% N, 9.3 wt.% O) to a highly pristine carbon surface (0.1 wt.% N, 0.3 wt.% O) without altering its pore morphology. Compared with N-CMS, the non-doped CMS contained a lower O content of 2.8 wt.%, and this gradually decreased to 2.5, 1.6, and 0.8 wt.% under high-temperature annealing at 1400, 1600, and 1800 °C, respectively (Figure 2f).

Figure 3a shows the X-ray diffraction (XRD) patterns of nitrogen-doped carbon materials, where the peak at $2\theta = 43°$

corresponds to the graphene in-plane diffraction. The index of (10) was used here instead of (100) because the structure was a two-dimensional lattice and the c-axis could not be defined.[63–65] Upon increasing the annealing temperature, the carbon (10) peak became more intense, suggesting an increase in the graphene domain size. Such a phenomenon was not observed in the undoped carbon materials (Figure S6a, Supporting Information), possibly due to the lower degree of heteroatom dopants in CMS. The domain size (L_a) was then determined from the full width at half maximum (FWHM) of the XRD (10) peak, as shown in Figure 3b. L_a was found to increase upon increasing the annealing temperature, implying that the graphene structure was gradually refined after the removal of the nitrogen dopants and oxygen functionalities during annealing. Figure 3c shows the Raman spectra of nitrogen-doped carbon materials. N-CMS exhibits a broad Raman G band, which gradually became narrower at higher annealing temperatures. As shown in Figure S7 (Supporting Information), the Raman spectra were deconvoluted into four bands,[13] the G band, the D band, the band ascribed to

**ADVANCED
SCIENCE NEWS**

www.advancedsciencenews.com

NANO · MICRO

small

www.small-journal.com

Figure 4. CV curves for a) the doped and b) the undoped carbon materials in an organic electrolyte composed of 1 M Et$_4$NBF$_4$/PC. The scan rate employed was 1 mV s^{-1}. The C_Q values obtained using the determined values of C_{areal} and C_H for c) the doped and d) the undoped carbon materials are shown (see details in the Supporting Information).

amorphous carbon (i.e., the Am band), and the band ascribed to the sp^3-bonded carbon atoms (i.e., the P band). The FWHM of the G-band (G-FWHM) gradually decreased as the annealing temperature increased (Figure 3d). This also indicated a refinement of the graphene structure and confirmed that the XRD and Raman results agreed with the XPS and CHN analyses described above. The calculated I_D/I_G ratio increases with annealing temperature (Figure S8, Supporting Information). The intense D band of N-GMS-1800 should be ascribed to the crystallite boundaries along the basal planes as explained in our previous work.[49]

Figure 4a,b show the CV curves of the nitrogen-doped and undoped carbon materials measured in a three-electrode cell using an organic electrolyte consisting of 1 M tetraethylammonium tetrafluoroborate dissolved in propylene carbonate (Et$_4$NBF$_4$/PC). The potential range was limited to between −1.1 and 0.5 V versus Ag/AgClO$_4$ so that the obtained CV curves (the first four cycles) were symmetrical to the x-axis (Figure 4a,b). Thus, the electrochemical process was highly reversible and free from irreversible reactions (an example is shown in Figure S9, Supporting Information), i.e., parasitic side reactions between carbon and the organic solvent molecules.[10,13] The CV curves of N-GMS-1000 and N-GMS-1200 exhibited a rectangular shape (Figure 4a), which is typical for the majority of carbon materials. However, when the annealing temperature was increased to above 1400 °C, the CV curves transformed from rectangular to butterfly-like shape (Figure 4a). Additionally, C_{tot} gradually decreased and the potential corresponding to the minimum C_{tot} gradually decreased with increasing annealing temperature

(Figure 4a). On the other hand, the undoped carbon materials exhibited butterfly-shaped CV curves similar to that of N-GMS-1800 (Figure 4b) regardless of the annealing at 1800 °C. CMS exhibited only a little higher C_{tot} than GMS-1800 (Figure 4b), indicating that the inclusion of H- and O-terminated edge sites (Figure 2f) in the minimally stacked graphene walls is not effective in enhancing C_{tot}. By contrast, the inclusion of H- and O-terminated edge sites together with N functionalities (Figure 2e) remarkably enhances C_{tot}.

3. Discussion

First, we discuss the decrease in C_{tot} with the increase in annealing temperature (Figure 4a,b). Generally, the decrease in C_{tot} can be attributed to the following possible reasons: (1) a decrease in the SSA;[8] (2) a decrease in the pore size;[36,66,67] (3) impaired wettability;[68,69] (4) reduced electrostatic interactions;[46] (5) a decrease in the pseudocapacitance. ;[9,44,70–73] or (6) a decrease in C_Q.[8,47] In the case of the N-GMS samples, we can rule out (1) and (2) because the porous structures of the annealed samples were largely identical as shown in Figure 1. For (3), we used an organic electrolyte together with mesoporous carbon materials. The pore sizes were significantly larger than the sizes of the solvent molecules and ions; therefore, the wettability was not likely to be adversely affected by high-temperature annealing.[74] For (4), C_H could decrease when O and N functionalities were lost by annealing and the carbon-ion interaction was weakened.[33,46] However, (4) cannot explain the transformation of the CV curves from

ADVANCED
SCIENCE NEWS
www.advancedsciencenews.com

NANO · MICRO
small
www.small-journal.com

rectangular to butterfly-shaped. For (5), some studies have ascribed the enhancement in C_{tot} for nitrogen-doped carbon materials to reversible reactions occurring between the surface functionalities and the aqueous electrolyte.[9,31,44,70–73] However, we used an organic electrolyte, which eliminates this scenario. Moreover, the shapes of the CV curves and the shift of the potential corresponding to the minimum C_{tot} value cannot be explained by pseudocapacitance. Thus, only (6) can explain the decrease in C_{tot}, the appearance of butterfly-shaped CV curves, and the shift of the potential corresponding to the minimum C_{tot} value.

To extract C_Q (see Equations (1–3) in Supporting Information), C_{tot} (F g^{-1}) was converted into C_{areal} (µF cm^{-2}) using the SSA of the carbon (Figure S10). While N-GMS-1000 exhibited the highest C_{areal} value of ≈6 µF cm^{-2}, the minimum C_{areal} value of N-GMS-1800 was ≈2.9 µF cm^{-2}. The areal C_H value was determined to be 9.7 µF cm^{-2} as reported in our previous work.[8] Subsequently, C_Q (µF cm^{-2}) was calculated using the obtained C_{areal} and C_H values (see details in the Supporting Information). As shown in Figure 4c, the C_Q of N-GMS-1000 was calculated to be in the range of 17–20 µF cm^{-2}, larger than the value of C_H (9.7 µF cm^{-2}, dashed orange line). By contrast, N-GMS-1800 showed a significantly smaller C_Q value with a minimum of ≈4.2 µF cm^{-2} and a slope of ≈21 µF cm^{-2} V^{-1} over the potential range of 0.3–0.4 V. For pure and perfect graphene, the theoretically calculated C_Q has a minimum value that is close to zero at the Dirac point and increases with potential with a slop of ≈23 µF cm^{-2} V^{-1} on each side of the Dirac point.[20] Xia et al. experimentally measured the C_Q of graphene exfoliated from Kish graphite by a tape and reported the minimum C_Q value to be ≈6.7 µF cm^{-2} and the slope to be ≈11 µF cm^{-2} V^{-1}.[20] The authors suggest such a difference between theoretical calculations and experimental results can be explained by the existence of impurities and defects in a real graphene structure.[20] Ruoff et al. reported a minimum C_Q value of ≈2.5 µF cm^{-2} and a slope of ≈22 µF cm^{-2} V^{-1} for graphene synthesized by methane CVD on a copper foil.[22] The C_Q of N-GMS-1800 is comparable to the results previously measured for graphene despite the differences in their dimensions and overall sizes. This is in good agreement with our previous finding that our 3D graphene materials synthesized by the templated method possess well-served 2D properties.[8] For nitrogen-doped graphene, Ruoff et al. reported a minimum C_Q value of ≈5.5 µF cm^{-2} and a slope of ≈16 µF cm^{-2} V^{-1}.[22] The difference between Ruoff's result and the result of N-GMS-1000 should be ascribed to the enhanced nitrogen doping amount in our case (4.5 wt.% vs 1.7 wt.% reported previously[22]). Based on these results, the transformation of the CV curve shape can be understood by considering that C_Q is enhanced to values larger than C_H when the carbon surface is highly functionalized. Since C_{tot}, C_H, and C_Q are related through the inverse sum, C_H becomes the dominant factor affecting C_{tot}. As C_H is relatively constant, the CV curve displayed a rectangular shape. When the carbon surface was defunctionalized, C_Q decreased to values smaller than C_H. Thus, the impact of C_Q on C_{tot} was significant, and the CV curve transformed into a butterfly shape. For the undoped species, we found that annealing at 1800 °C reduced C_Q (Figure 4d). However, such a decrease was insignificant compared to that observed for the nitrogen-doped species.

To elucidate the mechanisms involved in the C_{tot} transition, we employed joint density functional theory (JDFT) simulations based on an implicit solvent model. We compared the C_{tot} and C_Q of pristine and nitrogen-doped graphene with varying amounts of graphitic nitrogen (1.6, 3.2, and 4.8 wt.%, the models are shown in **Figure 5a–d**. As shown in Figure 5e–h, there was a shift in the minimum C_{tot} to lower potentials with a reduced amount of graphitic nitrogen, which agreed with the experimental results (Figure 4a,c). From the theoretical results, we only found a negligible change in the shape of the C_{tot} curve with no transition from butterfly to rectangular-shaped transition, suggesting that merely introducing graphitic N did not effectively enhance C_Q. From the experimental results shown in Figure 4b,d, we found that oxygen functionalities did not effectively enhance C_{tot} or C_Q. Therefore, we deduced that the enhanced value of C_Q can be attributed to the N functionalities that were abundant below 1200 °C (pyrrolic N and pyridinic N) or their interactions with the H-terminated edge sites and oxygen functional groups.

To further confirm this assumption, two hole-containing models were used as shown in Figure S11a,b (Supporting Information). Model 1 was used as a reference, and Model 2 (9.4 wt.% N, 8.4 wt.% O) represented the structure of N-CMS (8.3 wt.% N, 9.3 wt.% O). For each model, we found an introduction of the density of states around the Fermi level (Figure S11c–e, Supporting Information), which would lead to an increase in C_Q. As Model 2 exhibited semi-conductor properties, we only calculated the C_{tot} curve for Model 1 as presented in Figure S12 (Supporting Information). As is evident, the curvature of C_{tot} followed that of the density of states (Figure S11d, Supporting Information) and we found an increase in the minimum of C_{tot} from ≈3.0 to ≈6.0 µF cm^{-2} with a much lower curvature. For our highly functionalized Model 2 (Figure S11e, Supporting Information) we expected an even higher C_{tot}. Therefore, we attributed the C_{tot} enhancement to the greater number of electronic states around the Fermi level compared to that of the pristine graphene (Figure S11, Supporting Information). These theoretical results were consistent with our previous conclusion that the change in magnitude of C_{tot} for the nitrogen-doped species shown in Figure 4a was due to the corresponding change in the C_Q component of C_{tot}. Many previous studies have reported that the rectangular CV curves of porous carbon materials arise from their metallic nature.[75] Such an explanation eliminates a C_Q-based theory for the majority of porous carbon materials. However, as demonstrated in this study, the rectangular CV curves did not necessarily imply the absence of C_Q. Instead, we posit that even for rectangular CV curves, C_{tot} can be further improved via C_Q enhancement.

4. Conclusion

In summary, nitrogen-doped graphene frameworks with an ultrahigh mesoporosity (≈2100 m^2 g^{-1}) were synthesized using a templating method. The framework was thermally stable and the pore structure was unchanged upon the annealing from 1000 to 1800 °C, while the graphene framework refined gradually and the incorporated nitrogen dopants and oxygen functionalities were systematically altered. In addition, nitrogen-free counterparts were also synthesized. These materials were used as model porous materials consisting of minimally stacked graphene walls with different amounts of H, O, and N to in-

ADVANCED
SCIENCE NEWS
www.advancedsciencenews.com

NANO · MICRO
small
www.small-journal.com
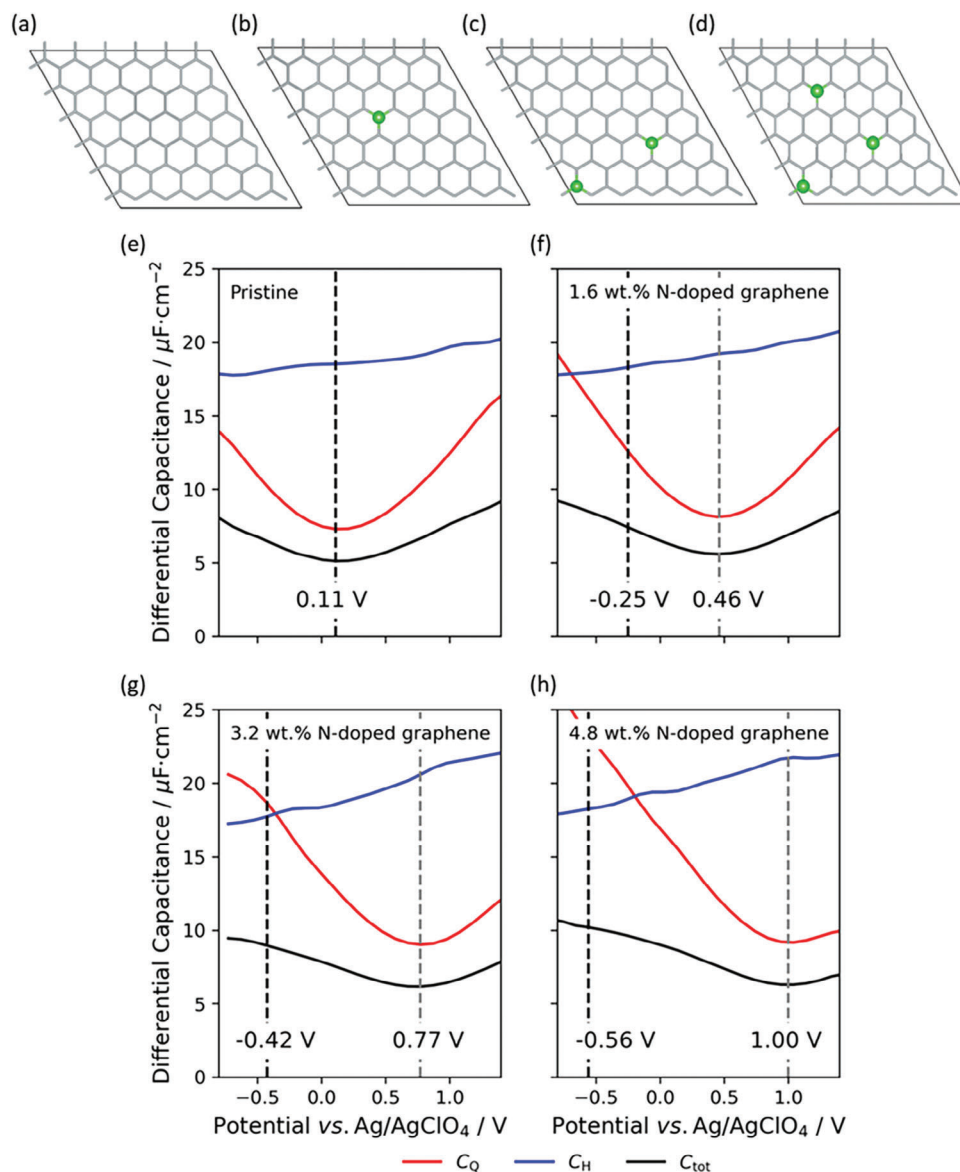
Figure 5. Periodic structural models of a) pristine graphene and nitrogen-doped graphene with varying amounts of graphitic nitrogen b) 1.6, c) 3.2, and d) 4.8 wt.%. Green dots indicate graphitic nitrogen in the carbon frameworks. Comparison of the calculated differential capacitances separated into their quantum and Helmholtz contributions for e) the pristine graphene and the f) 1.6 wt.%, g) 3.2 wt.%, and h) 4.8 wt.% N-doped graphene surfaces. The dashed black and gray dotted lines indicate the calculated PZC and the minimum C_Q, respectively.

vestigate the impact of the heteroatoms on their capacitive behavior. The value of C_{tot} was found to decrease upon increasing the annealing temperature, and the CV curves gradually transformed from rectangular to butterfly-shaped curves. We propose that the decrease in C_{tot} was due to the defunctionalizing of carbon frameworks, which resulted in a decrease in C_Q. Our results indicated that C_Q was enhanced to values larger than C_H when the carbon surface was highly functionalized, which leads to the smaller component (C_H) significantly affecting the value of C_{tot}, moreover, the values of C_H were relatively constant, thus producing a rectangular CV curve. Overall, this work potentially expands the scope of future research leading to a better understanding of the nature

of C_Q. It also broadens the scope of applications of C_Q theory to various materials ranging from graphene to its three-dimensional frameworks, which is important in the design of desirable carbon structures for supercapacitor applications. The model carbon materials presented here may also be useful in studies on the mechanism of other carbon-related electrochemical applications.[59,76–79]

Supporting Information

Supporting Information is available from the Wiley Online Library or from the author.

[1] F. Béguin, V. Presser, A. Balducci, E. Frackowiak, *Adv. Mater.* **2014**, *26*, 2219.

[2] P. Simon, Y. Gogotsi, *Nat. Mater.* **2020**, *19*, 1151.

[3] A. G. Olabi, Q. Abbas, A. Al Makky, M. A. Abdelkareem, *Energy* **2022**, *248*, 123617.

[4] M. E. Şahin, F. Blaabjerg, A. Sangwongwanich, *Energies* **2022**, *15*, 674.

[5] M. D. Stoller, S. Park, Y. Zhu, J. An, R. S. Ruoff, *Nano Lett.* **2008**, *8*, 3498.

[6] J. Wu, *Chem. Rev.* **2022**, *122*, 10821.

[7] G. Jeanmairet, B. Rotenberg, M. Salanne, *Chem. Rev.* **2022**, *122*, 10860.

[8] R. Tang, K. Nomura, K. Inoue, M. Kotani, T. Kyotani, H. Nishihara, *Electrochim. Acta* **2022**, *429*, 141009.

[9] S. Ghosh, S. Barg, S. M. Jeong, K. (K.) Ostrikov, *Adv. Energy Mater.* **2020**, *10*, 2001239.

[10] R. Tang, M. Yamamoto, K. Nomura, E. Morallón, D. Cazorla-Amorós, H. Nishihara, T. Kyotani, *J. Power Sources* **2020**, *457*, 228042.

[11] M. Thommes, K. Kaneko, A. V. Neimark, J. P. Olivier, F. Rodriguez-Reinoso, J. Rouquerol, K. S. W. Sing, *Pure Appl. Chem.* **2015**, *87*, 1051.

[12] W. Yu, T. Yoshii, A. Aziz, R. Tang, Z.-Z. Pan, K. Inoue, M. Kotani, H. Tanaka, E. Scholtzová, D. Tunega, Y. Nishina, K. Nishioka, S. Nakanishi, Y. Zhou, O. Terasaki, H. Nishihara, *Adv. Sci. (Weinh)* **2023**, *10*, e2300268.

[13] R. Tang, K. Taguchi, H. Nishihara, T. Ishii, E. Morallón, D. Cazorla-Amorós, T. Asada, N. Kobayashi, Y. Muramatsu, T. Kyotani, *J. Mater. Chem. A* **2019**, *7*, 7480.

[14] J.-P. Randin, E. Yeager, *J. Electrochem. Soc.* **1971**, *118*, 711.

[15] J.-P. Randin, E. Yeager, *J. Electroanal. Chem. Interfacial Electrochem.* **1972**, *36*, 257.

[16] H. Gerischer, *J. Phys. Chem.* **1985**, *89*, 4249.

[17] O. Barbieri, M. Hahn, A. Herzog, R. Kötz, *Carbon* **2005**, *43*, 1303.

[18] M. Hahn, M. Baertschi, O. Barbieri, J.-C. Sauter, R. Kötz, R. Gallay, *Electrochem. Solid-State Lett.* **2004**, *7*, A33.

[19] P. W. Ruch, R. Kötz, A. Wokaun, *Electrochim. Acta* **2009**, *54*, 4451.

[20] J. Xia, F. Chen, J. Li, N. Tao, *Nat. Nanotechnol.* **2009**, *4*, 505.

[21] M. D. Stoller, C. W. Magnuson, Y. Zhu, S. Murali, J. W. Suk, R. Piner, R. S. Ruoff, *Energy Environ. Sci.* **2011**, *4*, 4685.

[22] L. L. Zhang, X. Zhao, H. Ji, M. D. Stoller, L. Lai, S. Murali, S. Mcdonnell, B. Cleveger, R. M. Wallace, R. S. Ruoff, *Energy Environ. Sci.* **2012**, *5*, 9618.

[23] E. Uesugi, H. Goto, R. Eguchi, A. Fujiwara, Y. Kubozono, *Sci. Rep.* **2013**, *3*, 1595.

[24] H. Ji, X. Zhao, Z. Qiao, J. Jung, Y. Zhu, Y. Lu, L. L. Zhang, A. H. Macdonald, R. S. Ruoff, *Nat. Commun.* **2014**, *5*, 3317.

[25] C. Zhan, D.-E. Jiang, *J. Phys. Chem. Lett.* **2016**, *7*, 789.

[26] B. Dyatkin, Y. Gogotsi, *Faraday Discuss.* **2014**, *172*, 139.

[27] J. Ye, Y.-C. Wu, K. Xu, K. Ni, N. Shu, P.-L. Taberna, Y. Zhu, P. Simon, *J. Am. Chem. Soc.* **2019**, *141*, 16559.

[28] C. T. Hsieh, H. Teng, *Carbon* **2002**, *40*, 667.

[29] D. Qu, *J. Power Sources* **2002**, *109*, 403.

[30] H. Itoi, H. Nishihara, T. Ishii, K. Nueangnoraj, R. Berenguer-Betrián, T. Kyotani, *Bull. Chem. Soc. Jpn* **2014**, *87*, 250.

[31] A. Castro-Muñiz, Y. Hoshikawa, T. Kasukabe, H. Komiyama, T. Kyotani, *Langmuir* **2016**, *32*, 2127.

[32] H. Itoi, H. Nishihara, T. Kyotani, *Langmuir* **2016**, *32*, 11997.

[33] C. Cui, Y. Gao, J. Li, C. Yang, M. Liu, H. Jin, Z. Xia, L. Dai, J. Wang, S. Wang, *Angew. Chem., Int. Ed.* **2020**, *59*, 7928.

[34] G. Salitra, A. Soffer, L. Eliad, Y. Cohen, D. Aurbach, *J. Electrochem. Soc.* **2000**, *147*, 2486.

[35] K. Kierzek, E. Frackowiak, G. Lota, G. Gryglewicz, J. Machnikowski, *Electrochim. Acta* **2004**, *49*, 515.

[36] J. Chmiola, G. Yushin, Y. Gogotsi, C. Portet, P. Simon, P. L. Taberna, *Science* **2006**, *313*, 1760.

[37] C. Largeot, C. Portet, J. Chmiola, P.-L. Taberna, Y. Gogotsi, P. Simon, *J. Am. Chem. Soc.* **2008**, *130*, 2730.

[38] S. Fleischmann, Y. Zhang, X. Wang, P. T. Cummings, J. Wu, P. Simon, Y. Gogotsi, V. Presser, V. Augustyn, *Nat. Energy* **2022**, *7*, 222.

[39] Y. M. Liu, C. Merlet, B. Smit, *ACS Cent. Sci.* **2019**, *5*, 1813.

[40] C. Prehal, C. Koczwara, N. Jäckel, A. Schreiber, M. Burian, H. Amenitsch, M. A. Hartmann, V. Presser, O. Paris, *Nat. Energy* **2017**, *2*, 16215.

[41] R. Futamura, T. Iiyama, Y. Takasaki, Y. Gogotsi, M. J. Biggs, M. Salanne, J. Ségalini, P. Simon, K. Kaneko, *Nat. Mater.* **2017**, *16*, 1225.

[42] S. Boukhalfa, D. Gordon, L. He, Y. B. Melnichenko, N. Nitta, A. Magasinski, G. Yushin, *ACS Nano* **2014**, *8*, 2495.

[43] G. Lota, B. Grzyb, H. Machnikowska, J. Machnikowski, E. Frackowiak, *Chem. Phys. Lett.* **2005**, *404*, 53.

[44] E. Frackowiak, G. Lota, J. Machnikowski, C. Vix-Guterl, F. Béguin, *Electrochim. Acta* **2006**, *51*, 2209.

[45] W. R. Li, D. H. Chen, Z. Li, Y. F. Shi, Y. Wan, G. Wang, Z. Y. Jiang, D. Y. Zhao, *Carbon* **2007**, *45*, 1757.

[46] H. M. Jeong, J. W. Lee, W. H. Shin, Y. J. Choi, H. J. Shin, J. K. Kang, J. W. Choi, *Nano Lett.* **2011**, *11*, 2472.

[47] J. Chen, Y. Han, X. Kong, X. Deng, H. J. Park, Y. Guo, S. Jin, Z. Qi, Z. Lee, Z. Qiao, R. S. Ruoff, H. Ji, *Angew. Chem., Int. Ed.* **2016**, *55*, 13822.

[48] C. Portet, Z. Yang, Y. Korenblit, Y. Gogotsi, R. Mokaya, G. Yushin, *J. Electrochem. Soc.* **2009**, *156*, A1.

[49] H. Nishihara, T. Simura, S. Kobayashi, K. Nomura, R. Berenguer, M. Ito, M. Uchimura, H. Iden, K. Arihara, A. Ohma, Y. Hayasaka, T. Kyotani, *Adv. Funct. Mater.* **2016**, *26*, 6418.

[50] Y. Qin, Z. Song, L. Miao, C. Hu, Y. Chen, P. Liu, Y. Lv, L. Gan, M. Liu, *Chem. Eng. J.* **2023**, *470*, 144256.

[51] Y. Zhang, Z. Song, L. Miao, Y. Lv, L. Gan, M. Liu, *ACS Appl. Mater. Interfaces* **2023**, *15*, 35380.

[52] Z. Song, L. Miao, Y. Lv, L. Gan, M. Liu, *Angew. Chem., Int. Ed.* **2023**, *62*, e202309446.

[53] M. Inagaki, M. Toyoda, T. Tsumura, *RSC Adv.* **2014**, *40*, 41411.

[54] K. Nomura, H. Nishihara, N. Kobayashi, T. Asada, T. Kyotani, *Energy Environ. Sci.* **2019**, *12*, 1542.

2308066 (9 of 10)

ADVANCED
SCIENCE NEWS

www.advancedsciencenews.com

NANO · MICRO
small
www.small-journal.com

[55] S. Sunahiro, K. Nomura, S. Goto, K. Kanamaru, R. Tang, M. Yamamoto, T. Yoshii, J. N. Kondo, Q. Zhao, A. Ghulam Nabi, R. Crespo-Otero, D. Di Tommaso, T. Kyotani, H. Nishihara, *J. Mater. Chem. A* **2021**, *9*, 14296.

[56] A. Maetz, L. Delmotte, G. Moussa, J. Dentzer, S. Knopf, C. M. Ghimbeu, *Green Chem.* **2017**, *19*, 2266.

[57] D. Guo, R. Shibuya, C. Akiba, S. Saji, T. Kondo, J. Nakamura, *Science* **2016**, *351*, 361.

[58] K. Lee, J. Lim, M. J. Lee, K. Ryu, H. Lee, J. Y. Kim, H. Ju, H.-S. Cho, B.-H. Kim, M. C. Hatzell, J. Kang, S. W. Lee, *Energy Environ. Sci.* **2022**, *15*, 2858.

[59] B. Hu, Y. Wu, K. Wang, H. Guo, Z. Lei, Z. Liu, L. Wang, *Small* **2023**, 2305344.

[60] Z. Liu, W. Hou, H. Guo, Z. Wang, L. Wang, M. Wu, *ACS Appl. Mater. Interfaces* **2023**, *15*, 33868.

[61] S. A. Chernyak, A. S. Ivanov, E. A. Arkhipova, A. V. Shumyantsev, N. E. Strokova, K. I. Maslakov, S. V. Savilov, V. V. Lunin, *Appl. Surf. Sci.* **2019**, *484*, 228.

[62] T. Kato, Y. Yamada, Y. Nishikawa, T. Otomo, H. Sato, S. Sato, *J. Mater. Sci.* **2021**, *56*, 15798.

[63] B. E. Warren, *Phys. Rev.* **1941**, *59*, 693.

[64] J. Biscoe, B. E. Warren, *J. Appl. Phys.* **1942**, *13*, 364.

[65] M. Inagaki, F. Kang, *Materials Science and Engineering of Carbon: Fundamentals*, Second Edition, Butterworth-Heinemann, Waltham **2014**.

[66] J. Huang, B. G. Sumpter, V. Meunier, *Angew. Chem., Int. Ed.* **2008**, *47*, 520.

[67] J. Huang, B. G. Sumpter, V. Meunier, *Chemistry* **2008**, *14*, 6614.

[68] J. Zhao, H. Lai, Z. Lyu, Y. Jiang, K. Xie, X. Wang, Q. Wu, L. Yang, Z. Jin, Y. Ma, J. Liu, Z. Hu, *Adv. Mater.* **2015**, *27*, 3541.

[69] L. Wan, J. Wang, L. Xie, Y. Sun, K. Li, *ACS Appl. Mater. Interfaces* **2014**, *6*, 15583.

[70] D. Hulicova, J. Yamashita, Y. Soneda, H. Hatori, M. Kodama, *Chem. Mater.* **2005**, *17*, 1241.

[71] T. Lin, I.-W. Chen, F. Liu, C. Yang, H. Bi, F. Xu, F. Huang, *Science* **2015**, *350*, 1508.

[72] Y.-H. Lee, K.-H. Chang, C.-C. Hu, *J. Power Sources* **2013**, *227*, 300.

[73] D. Hulicova-Jurcakova, M. Seredych, G. Q. Lu, T. J. Bandosz, *Adv. Funct. Mater.* **2009**, *19*, 438.

[74] H. Nishihara, H. Itoi, T. Kogure, P.-X. Hou, H. Touhara, F. Okino, T. Kyotani, *Chem. - Eur. J.* **2009**, *15*, 5355.

[75] F. Béguin, E. Frackowiak, *Supercapacitors: Materials, Systems, and Applications*, Wiley-VCH, Zurich **2013**.

[76] X. Shen, Z. Wang, H. Guo, Z. Lei, Z. Liu, L. Wang, *Small* **2023**, *19*, 2303156.

[77] Z. Wang, G. Li, W. Hou, H. Guo, L. Wang, M. Wu, *ACS Nano* **2023**, *17*, 8671.

[78] R. M. Yadav, Z. Li, T. Zhang, O. Sahin, S. Roy, G. Gao, H. Guo, R. Vajtai, L. Wang, P. M. Ajayan, J. Wu, *Adv. Mater.* **2022**, *34*, 2105690.

[79] M. Fan, Z. Wang, K. Sun, A. Wang, Y. Zhao, Q. Yuan, R. Wang, J. Raj, J. Wu, J. Jiang, L. Wang, *Adv. Mater.* **2023**, *35*, 2209086.